

The impact of microscale physics in continuous time random walks for hydrodynamic dispersion in disordered media

Xiangnan Yu,^{1,2} Marco Dentz,^{2,*} HongGuang Sun,¹ and Yong Zhang³

¹*The National Key Laboratory of Water Disaster Prevention,
College of Mechanics and Materials,
Hohai University, Nanjing 211100, China.*

²*Spanish National Research Council (IDAEA-CSIC), Barcelona, Spain.*

³*Department of Geological Sciences,
University of Alabama, Tuscaloosa, AL, USA.*

Abstract

The continuous time random walk (CTRW) approach has been widely applied to model large-scale non-Fickian transport in the flow through disordered media. Often, the underlying microscopic transport mechanisms and disorder characteristics are not known, and their effect on large-scale solute dispersion is encoded by a heavy-tailed transition time distribution. Here we study how the microscale physics manifests in the CTRW framework, and how it affects solute dispersion. To this end, we consider transport in disordered media with random sorption and random flow properties. Both disorder mechanisms can give rise to anomalous particle transport. We present the CTRW models corresponding to each of these physical scenarios to discuss the different manifestations of microscale heterogeneity on large-scale dispersion depending on the particle injection modes. The combined impact of random sorption and advection is studied with a novel CTRW model that explicitly represents both microscale disorder mechanisms. While random advection and sorption may show similar large-scale transport behaviors, they can be clearly distinguished in their response to uniform injection conditions, and, in general, to initial particle distributions that are not flux-weighted. These findings highlight the importance of the microscale physics for the interpretation and prediction of anomalous dispersion phenomena in disordered media.

* E-mail: marco.dentz@csic.es

I. INTRODUCTION

Solute transport in disordered media may be non-Fickian or anomalous. Anomalous dispersion manifests in nonlinear growth of the spatial variance of the solute distribution in time, backward and forward tails in spatial solute distributions and early and late solute arrival times. This type of behavior has been observed in experiments and detailed numerical simulations in porous media at the pore [1–5] and continuum scales [6–11], at the fracture and fracture network scales [12–15]. They can be traced back to broad distributions of characteristic mass transfer times, which impart a long memory and thus give rise to temporal non-locality. This is because the concentration distribution at a given time receives contributions of solute fluxes from a broad range of previous times unlike Fickian or Markovian transport models, which depend on the system state at one previous instant.

The mechanisms that can lead to non-local transport behaviors are for example sorption to the solid matrix [16, 17] and diffusion between regions of high flow velocity and stagnant regions [18, 19]. Non-Fickian behavior can also be induced by broad distributions of flow velocities. Steady flow through heterogeneous porous media is organized on the spatial scales imprinted in the medium structure, that is, Eulerian and Lagrangian velocities vary on characteristic length scales [20]. Thus, broad distributions of flow velocities induce broad distributions of advective mass transfer times. Spatio-temporal non-locality may be caused by preferential flow paths in single fractures [21], strongly correlated hydraulic conductivity fields [22], and channelling flow in unconfined alluvial aquifers [8].

As a result of the ubiquity of anomalous solute dispersion, non-Fickian transport models have received growing attention in the last three decades. Several alternative approaches were proposed to quantify non-Fickian flow and transport behaviors [23–26], such as fractional advection-dispersion equations (FADE) [27–29], the multi-rate mass transfer (MRMT) approach [19], and continuous time random walk (CTRW) [25] and time-domain random walk (TDRW) [30, 31] approaches. A review of random walk methods for modeling of transport in heterogeneous media can be found in [23]. These modeling approaches are motivated by the phenomenologies for anomalous transport discussed above, and account for broad distributions of mass transfer times. Oftentimes, however, the microscopic disorder or transport mechanisms are not known, or there may be a combination of different mechanisms that lead to non-local behavior.

We address the questions of how microscale transport and disorder characteristics impact on large-scale dispersion, and whether and under which conditions it is possible to distinguish between different microscale transport mechanisms from large scale observations. To this end, we use the CTRW approach to quantify different microscale disorder mechanisms and analyze the resulting large-scale transport behaviors. In general, the CTRW approach represents the impact the medium heterogeneity and microscopic transport mechanisms in terms of a distribution of characteristic mass transfer times, specifically the transition or waiting time distribution [25]. The latter have been modeled based on power-law or truncated power-law distributions [25], which are flexible but often lack a direct relation with the underlying heterogeneity. However, CTRW models have also been used for the upscaling of dispersion in porous and fractured media in terms of medium geometry and heterogeneity statistics [11, 14, 32, 33]. We use the CTRW here in the latter sense as an upscaling framework that allows us to explicitly represent microscale disorder and transport mechanisms. Thus, we consider the CTRW models that describe transport under spatially random sorption (RS) and random advection (RA) properties, and analyze their impact on the large-scale transport signatures for different initial solute distributions. Based on this approach, we furthermore derive a novel CTRW model that explicitly represents both disorder mechanisms and analyze the combined impact of random sorption and advection (RSA) properties on large-scale dispersion. We find that transport under random sorption and random advection may show similar large-scale dispersion behaviors, but they can be clearly distinguished in terms of their response to different initial conditions. These features persist and can be identified also under the combined effect of random sorption and advection.

The paper is organized as follows. Section II presents three CTRW models that are derived from different microscale transport mechanisms, namely spatially random sorption, incompressible spatial random flow, and the combination of both. For each model, both flux-weighted and uniform injection modes are considered. The transport behaviors in these models are analyzed by numerical random walk simulations and in terms of analytical expressions for the early and long time asymptotics in Section III.

II. TRANSPORT MODELS

In this section, we present the microscale models that describe transport under random sorption and advection. We first formulate the CTRW models that represent each disorder mechanism separately, namely the random sorption (RS) and random advection (RA) models. We follow here the approaches in Refs. [20, 34]. Then we derive the CTRW model that explicitly represents the combination of both disorder mechanisms (RSA). In all cases, we start from the respective microscale transport descriptions. Afterward, we formulate the corresponding stochastic time-domain random walk and continuous time random walk models.

A. Random sorption (RS)

We consider advective transport under linear equilibrium sorption in constant flow. Mass conservation for the total solute concentration $c(x, t)$ is described by [34]:

$$\frac{\partial c(\mathbf{x}, t)}{\partial t} = -\mathbf{v}_0 \cdot \nabla c_m(\mathbf{x}, t), \quad (1)$$

where $c_m(\mathbf{x}, t)$ is the non-adsorbed, mobile concentration. We disregard here diffusion. The flow velocity \mathbf{v}_0 represents constant flow, and, as a result, the transport in this model is not sensitive to the way in which the solute is injected. This is discussed in more detail in Section II D. The total concentration is given in terms of $c_m(\mathbf{x}, t)$ and the adsorbed, immobile concentration $c_{im}(x, t)$ as:

$$c(\mathbf{x}, t) = \theta c_m(\mathbf{x}, t) + (1 - \theta)c_{im}(\mathbf{x}, t), \quad (2)$$

where θ is the effective porosity. The immobile concentration is related to the mobile concentration through the spatially varying distribution coefficient $k(x)$ [35],

$$c_{im}(\mathbf{x}, t) = k(\mathbf{x})c_m(\mathbf{x}, t). \quad (3)$$

Inserting equations (2) and (3) into equation (1), one obtains the governing equation for the mobile concentration:

$$R(\mathbf{x}) \frac{\partial c_m(\mathbf{x}, t)}{\partial t} = -\mathbf{v}_0 \cdot \nabla c_m(\mathbf{x}, t), \quad (4)$$

where we define the retardation factor $R(\mathbf{x}) = \theta + (1 - \theta)k(\mathbf{x})$. The total concentration $c(\mathbf{x}, t)$ describes the equation

$$\frac{\partial c(\mathbf{x}, t)}{\partial t} = -\mathbf{v}_0 \cdot \nabla \frac{c(\mathbf{x}, t)}{R(\mathbf{x})}. \quad (5)$$

In the following, we assume that the constant flow velocity is aligned with the x -direction of the coordinate system such that $\mathbf{v}_0 = v_0 \mathbf{e}_x$, where \mathbf{e}_x is the unit vector in x -direction. Solute transport can be described equivalently in terms of the following kinematic equation for the particle position $x(t)$,

$$dx(t) = \frac{v_0 dt}{R[x(t)]}. \quad (6)$$

1. Continuous time random walk model

In order to derive the equivalent continuous time random walk model, we define now $d\tau = dt/R[x(t)]$ and write Equation (6) as

$$dx(\tau) = v_0 d\tau \qquad dt = R(x) d\tau \quad (7)$$

We assume that the random retardation factor $R(x)$ is piecewise constant over the distances ξ . The distribution of ξ in the following is denoted by $\rho(x)$. We employ here the exponential distribution

$$\rho(x) = \ell_c^{-1} \exp(-x/\ell_c), \quad (8)$$

with the characteristic length scale ℓ_c . The characteristic advection time is defined by $\tau_c = \ell_c/v_0$. The single-point distribution of $R(x)$ is denoted by $p_R(r)$. The equation of motion (7) can then be coarse-grained on the lengths ξ as [34]

$$x_{n+1} = x_n + \xi_n, \qquad t_{n+1} = t_n + \tau_n, \quad (9)$$

where the transition time is given by $\tau_n = \xi_n R_n / v_0$.

The joint distribution of transition length and time is given by

$$\psi(x, t) = \rho(x) \frac{v_0}{x} p_R(v_0 t / x), \quad (10)$$

The transition time distribution is given by

$$\psi(t) = \int_{-\infty}^{\infty} dx \rho(x) \frac{v_0}{x} p_R(v_0 t / x). \quad (11)$$

As $\rho(x)$ is localized at around $x = \ell_c$, we can approximate $\psi(t)$ as

$$\psi(t) \approx \frac{v_0}{\ell_c} p_R(v_0 t / \ell_c). \quad (12)$$

The stochastic Langevin model (9) is equivalent to the following generalized master equation for the particle density $p(x, t)$ [25]

$$\frac{\partial p(x, t)}{\partial t} = \int dx \int_0^t dt' \mathcal{K}(x - x', t - t') [c(x', t') - c(x, t')], \quad (13)$$

where the memory kernel $\mathcal{K}(x, t)$ is given in Laplace space by

$$\mathcal{K}^*(x, \lambda) = \frac{\lambda \psi^*(x, \lambda)}{1 - \psi^*(\lambda)}. \quad (14)$$

B. Random advection (RA)

The random advection model describes advective transport in the incompressible flow through a heterogeneous porous medium. The tracer concentration satisfies

$$\frac{\partial c(\mathbf{x}, t)}{\partial t} + \mathbf{u}(\mathbf{x}) \cdot \nabla c(\mathbf{x}, t) = 0. \quad (15)$$

where $\mathbf{u}(\mathbf{x})$ is steady divergence-free random velocity field in a porous medium. Spatial fluctuations can be due to variability in the geometry of the pore space for pore-scale flow and transport [5] or spatially varying hydraulic conductivity on the continuum scale [11]. The Liouville equation (15) is equivalent to the following kinematic equation for the position $\mathbf{x}(t)$ of a tracer particle

$$d\mathbf{x}(t) = \mathbf{u}[\mathbf{x}(t)] dt. \quad (16)$$

The travel distance $s(t)$ along a streamline is given by

$$ds(t) = |\mathbf{u}[\mathbf{x}(t)]| dt. \quad (17)$$

The variable change $t \rightarrow s$ in (16) gives for the streamwise particle position [11, 20]

$$dx(s) = ds/\chi, \quad dt(s) = 1/v(s), \quad (18)$$

where we defined $v(s) = |\mathbf{u}[\mathbf{x}(s)]|$, and approximated $u_1[\mathbf{x}(s)]/v(s) = 1/\chi$ with $\chi = \bar{v}/\bar{u}_1$ advective tortuosity. In the following we set $\chi = 1$ for simplicity. The distribution $p_v(v)$ of

flow speeds $v(s)$ along streamlines is related to the distribution $p_e(v)$ of Eulerian flow speeds by [20]

$$p_v(v) = \frac{vp_e(v)}{\langle v_e \rangle}. \quad (19)$$

1. Stochastic time-domain random walk model

Following [20], we employ a Bernoulli process for the evolution of particle speeds $v(s)$ along streamlines. That is, the series $\{v(s)\}$ of particle speeds is generated by the following stochastic relaxation process

$$v(s + ds) = v(s)[1 - \xi(s)] + \xi(s)\nu(s), \quad (20)$$

where $\nu(s)$ is distributed according to $p_v(v)$, and $\xi(s)$ is a Bernoulli variable which is equal to one with probability $\exp(-ds/\ell_c)$ and zero else. The probability for a transition from $v(s') = v'$ to $v(s) = v$ is then

$$p_v(v, s - s' | v') = \exp[-(s - s')/\ell_c] \delta(v - v') + (1 - \exp[-(s - s')/\ell_c]) p_v(v), \quad (21)$$

where ℓ_c denotes the variation scale of $v(x)$. The distribution of initial particle velocities is denoted by $p_0(v)$. The joint density $p(x, v, t)$ of particle position and speed is governed by the Boltzmann-type equation [11, 36]

$$\frac{\partial p(x, v, t)}{\partial t} + v \frac{\partial p(x, v, t)}{\partial x} = -\frac{v}{\ell_c} p(x, v, t) + p_v(v) \int_0^\infty dv' \frac{v'}{\ell_c} p(x, v', t). \quad (22)$$

We consider the initial distribution $p(x, v, t = 0) = \delta(x)p_0(v)$.

2. Continuous time random walk model

In order to see the correspondence between the RA and RS models, we determine the equivalent CTRW model by coarse-graining the equations of motion (18). To this end, we note that the Bernoulli process given by Eq. (20) implies that the persistence lengths ξ of particle velocities are exponentially distributed, that is, their distribution $\rho(x)$ follows (8). This can be seen as follows. The probability p_n that the velocity does not change after n steps is

$$p_n = \exp[-nds/\ell_c]. \quad (23)$$

The latter is equal to the probability that the velocity remains constant for a distance larger than $x_n = nds$. This means that

$$\sum_{j=n}^{\infty} ds \rho(x_n) = \exp(-x_n/\ell_c). \quad (24)$$

In the continuum limit $n \rightarrow \infty$ and $ds \rightarrow 0$ such that $x_n \rightarrow x$, we see that $\rho(x)$ is the exponential distribution with characteristic scale ℓ_c . Thus, in analogy to Section II A, particle motion can be coarse-grained as

$$x_{n+1} = x_n + \xi_n, \quad t_{n+1} = t_n + \tau_n, \quad (25)$$

where the transition time is $\tau_n = \xi_n/v_n$. The joined distribution of transition lengths and time for $n > 0$ then is given by

$$\psi(x, t) = \rho(x) \frac{x}{t^2} p_v(x/t), \quad (26)$$

where $\rho(x)$ is given by (8). The transition time distribution $\psi_0(x, t)$ for the first CTRW step, that is, $n = 0$, is given in terms of the initial speed distribution as

$$\psi_0(x, t) = \rho(x) \frac{x}{t^2} p_0(x/t). \quad (27)$$

For $\psi_0(x, t) = \psi(x, t)$, the governing equation for the particle density $p(x, t)$ in this picture is identical to Eq. (13). Similar to Eq. (12), we can approximate the transition time distribution $\psi(t)$ as

$$\psi(t) \approx \frac{\ell_c}{t^2} p_v(\ell_c/t), \quad (28)$$

and analogously for $\psi_0(t)$. Aquino and Velásquez-Parra [37] studied the equivalence of the stochastic TDRW model and its coarse-grained counterpart.

C. Random sorption and advection (RSA)

Anomalous dispersion may be driven by multiple factors. Here we combine the sorption and velocity models into the random sorption and advection (RSA) model. The evolution of the total solute concentration $c(\mathbf{x}, t)$ is governed by

$$\frac{\partial c(\mathbf{x}, t)}{\partial t} + \mathbf{u}(\mathbf{x}) \cdot \nabla \frac{c(\mathbf{x}, t)}{R(\mathbf{x})} = 0. \quad (29)$$

The corresponding kinematic equation is

$$d\mathbf{x}(t) = -\frac{\mathbf{u}[\mathbf{x}(t)]dt}{R[\mathbf{x}(t)]}. \quad (30)$$

As in the previous section, we consider the distance $s(t)$ traveled along a streamline,

$$ds(t) = |\mathbf{u}[\mathbf{x}, t]| \frac{dt}{R[\mathbf{x}(t)]}. \quad (31)$$

The variable change $t \rightarrow s$ gives now for the streamwise particle position the equation

$$dx(s) = \chi^{-1}ds, \quad dt(s) = \frac{R(s)ds}{v(s)}. \quad (32)$$

As above, in the following we set $\chi = 1$ for simplicity.

1. Stochastic time-domain random walk model

We assume that $v(s)$ and $R(s)$ vary on the same length scale ℓ_c , and represent the series $\{v(s), R(s)\}$ as a joint Bernoulli process, that is, both evolve simultaneously according to Eqs. (20)-(21). The joint distribution of particle position, velocity and retardation coefficient $p(x, v, r, t)$ follows the Boltzmann type equation

$$\begin{aligned} \frac{\partial p(x, v, r, t)}{\partial t} + \frac{v}{r} \frac{\partial p(x, v, r, t)}{\partial x} = \\ - \frac{v}{r\ell_c} p(x, v, r, t) + p_v(v)\psi_R(r) \int_0^\infty dv' \int_0^\infty dr' \frac{v'}{r'\ell_c} p(x, v', r', t), \end{aligned} \quad (33)$$

see A. We consider the initial conditions $p(x, v, r, t = 0) = \delta(x)p_0(v)p_R(r)$.

2. Continuous time random walk model

As in the previous section, we derive now the equivalent CTRW model by coarse-graining the kinematic equations (32) on the correlation scale ℓ_c of $R(s)$ and $v(s)$. Thus, we obtain

$$x_{n+1} = x_n + \xi_n, \quad t_{n+1} = t_n + \tau_n, \quad (34)$$

where the transition time is now given by $\tau_n = R_n \xi_n / v_n$. The joint distribution $\psi(x, t)$ of transition length and time for $n > 0$ can be written as

$$\psi(x, t) = \rho(x) \int_0^\infty dv \frac{v}{x} p_v(v) p_R(vt/x) \quad (35)$$

For the first step, that is, $n = 0$, the distribution $\psi_0(x, t)$ is analogous to Eq. (35) with $p_v(v) \rightarrow p_0(v)$. Similar to Eqs. (12) and (28), we can approximate

$$\psi(t) \approx \int_0^{\infty} dv \frac{v}{\ell_c} p_v(v) p_R(vt/\ell_c) \quad (36)$$

and analogously for $\psi_0(t)$.

For $\psi_0(x, t) = \psi(x, t)$, the governing equation for the particle distribution $p(x, t)$ is given by Eq. (13). Under this condition, the RS, RA and RSA models have the same governing equations. The microscale heterogeneity and transport model determines the transition time distribution, and, as we will see in the following, the initial condition of the respective stochastic TDRW and CTRW models.

D. Initial conditions

The models discussed in the previous sections describe advective particle motion in heterogeneous media characterized by chemical and physical medium heterogeneities. These heterogeneities are represented by the spatially varying retardation coefficient $R(\mathbf{x})$ and flow speed $v(\mathbf{x})$. The initial conditions of the respective stochastic TDRW and CTRW models depend on the microscale physics, and are determined by the way particles are released in the medium. To illustrate this, we consider two particle injection scenarios, uniform and flux-weighted, which have been studied for solute transport in heterogeneous porous and fractured media [38–40]. In the first scenario, particles are released uniformly in space over a medium cross-section. In the second scenario, particles are injected across a medium cross-section proportional to the local flow speed. While the three CTRW models under consideration have similar or identical governing equations for certain initial conditions, the model behaviors are in general different.

For the RS model, there is no difference between the uniform and flux-weighted initial conditions because the flow velocity v_0 is constant. The CTRW model represents the stochastic dynamics of transport due to spatial variability in the retardation coefficient $R(x)$. For the RA and RSA models, the injection conditions are reflected in the distribution $p_0(v)$ of initial particle speeds. For the uniform injection condition, it is

$$p_0(v) = p_e(v). \quad (37)$$

For the flux-weighted injection condition, the initial speed distribution is

$$p_0(v) = \frac{vp_e(v)}{\langle v_e \rangle} = p_v(v). \quad (38)$$

In the following, we will analyze the transport behaviors in the different disorder models, and the impact of the underlying microscale physics.

III. TRANSPORT BEHAVIORS

In this section, we investigate the transport behaviors in the three stochastic models presented in the previous section, which account for transport under random sorption (RS), under random advection (RA), and under the impact of random sorption and advection (RSA). The transport behaviors are analyzed in terms of the displacement mean and variance, which are defined as

$$m(t) = \langle x(t) \rangle, \quad \kappa(t) = \langle x(t)^2 \rangle - \langle x(t) \rangle^2, \quad (39)$$

where the angular brackets denote the average over all particles. These quantities measure the time evolution of the center of mass of a particle plume and its spatial extension. In order to characterize the spatial distribution, we consider snapshots of the particle density, which is defined by

$$p(x, t) = \langle \delta[x - x(t)] \rangle. \quad (40)$$

Another quantity of interest in the distribution of arrival times at a control location, the particle breakthrough curve. The breakthrough time at a location x is defined by

$$t(x) = \min[t | x(t) \geq x]. \quad (41)$$

The arrival time distribution is defined by

$$f(t, x) = \langle \delta[t - t(x)] \rangle. \quad (42)$$

In the following, we first highlight the impact of microscale physical heterogeneity by comparison of the RA and RS models. Then we analyze the combined impact of the two microscale disorder mechanisms in the novel RSA model. The model behaviors are obtained from the numerical solution of the CTRW model of Section II A 1 for the RS model, and the stochastic time-domain random walk models of Sections II B 1 and II C 1.

A. Transport in the RA and RS models

In order to highlight the impact of the microscale physics on the expected transport behaviors in the RA and RS models, we consider disorder distributions that give rise to identical transition time distributions $\psi(t)$ in the two models. Specifically, in the RA model, we employ a Gamma distribution for the Eulerian flow speeds [20],

$$p_e(v) = \left(\frac{v}{v_0}\right)^{\alpha-1} \frac{\exp(-v/v_0)}{v_0\Gamma(\alpha)} \quad (43)$$

where $0 < \alpha < 1$. For the distribution of retardation coefficients in the RS model, we employ the inverse Gamma distribution

$$p_R(r) = \left(\frac{r}{r_0}\right)^{-1-\gamma} \frac{\exp(-r_0/r)}{r_0\Gamma(\gamma)}, \quad (44)$$

where $0 < \gamma < 2$. These distributions give rise to the following transition time distribution in both the RA and RS models

$$\psi(t) = \left(\frac{t}{\tau_0}\right)^{-1-\beta} \frac{\exp(-\tau_0/t)}{\tau_0\Gamma(\beta)}, \quad (45)$$

where $\tau_0 = \ell_c r_0 / v_0$ in the RS model, and $\tau_0 = \ell_c / v_0$ in the RA model. Furthermore, the exponent β corresponds to $\beta = \gamma$ in the RS and $\beta = \alpha + 1$ in the RA model. Note that we use here the approximate expressions (12) and (28) for $\psi(t)$.

As a first difference between the RS and RA models, we note that the exponent β in $\psi(t)$ for the RS model is bound between zero and two, $0 < \beta < 2$, while for the RA model it is between one and two, $1 < \beta < 2$. The latter is due to the relation (19) between the Eulerian and Lagrangian speed distributions, which is a result of the solenoidal character of the underlying flow field [20]. The distribution $\psi_0(t)$ of the first transition time τ_0 in the RS model is equal to $\psi(t)$ for both injection conditions because it depends only on the distribution $p_R(r)$ of the retardation factor, see (11). For the RA model, $\psi_0(t) = \psi(t)$ for the flux-weighted injection. For the uniform injection, it is given by Eq. (27) in terms of the initial speed distribution $p_0(v)$. Thus, the transition time distribution for the first CTRW step is given by

$$\psi_0(t) = \left(\frac{t}{\tau_0}\right)^{-1-\beta_0} \frac{\exp(-\tau_0/t)}{\tau_0\Gamma(\beta_0)}, \quad (46)$$

where $\beta_0 = \gamma$ and $\beta_0 = \alpha + 1$ for the flux-weighted injection in the RS and RA models, and $\beta_0 = \beta$ and $\beta_0 = \alpha$ for the uniform injection.

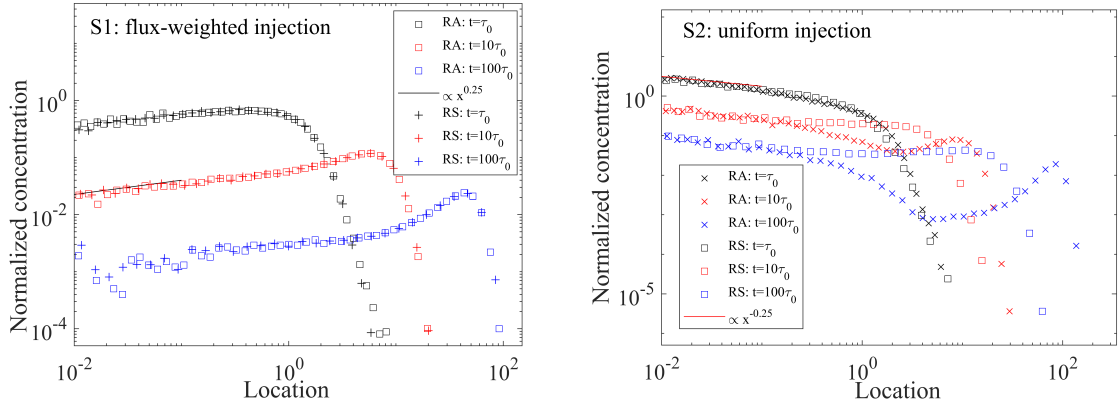


FIG. 1. Spatial particle profiles at time (black) $t = \tau_0$, (red) $t = 10\tau_0$ and (blue) $t = 100\tau_0$ for (top row) scenario S1 ($\gamma = 1.25$ and $\alpha = 0.25$) under flux-weighted injection, and (bottom row) scenario S2 ($\gamma = 0.75$ and $\alpha = 0.75$) under uniform injection. The crosses denote the RS model, the squares the RA model.

We consider in the following two scenarios. The first scenario (S1) sets $\gamma = \alpha + 1$, specifically, we use $\alpha = 1/4$. Thus, scenario S1 is characterized by the same $\psi(t)$ for both models, but different $\psi_0(t)$ under uniform injection. Scenario S2 sets $\gamma = \alpha$, specifically, we use $\alpha = 3/4$. This scenario is characterized by the same $\psi_0(t)$ for both models under uniform injection, but different $\psi(t)$. In the following, we consider scenario S1 for flux-weighted and scenario S2 for uniform injection conditions.

1. Spatial profiles

Figure 1 shows spatial profiles $p(x, t)$ at times $t = \tau_0, 10\tau_0$ and $100\tau_0$ for the RS and RA models for scenario S1 under flux-weighted and scenario S2 under uniform injection conditions. The profiles for the RS and RA models are indistinguishable in scenario S1. In fact, the two models are identical as shown in Section II B. The profiles are characterized by a backward tail and a leading edge. For scenario S2, the RS and RA profiles align at short times because the transition time distributions corresponding to the first CTRW step are the same. With increasing time, the peak at the origin erodes in both RS and RA and the behavior close to the origin remain similar. However, the spatial profiles in the RA model develop a second peak at the leading edge that advances much faster than in the RS model.

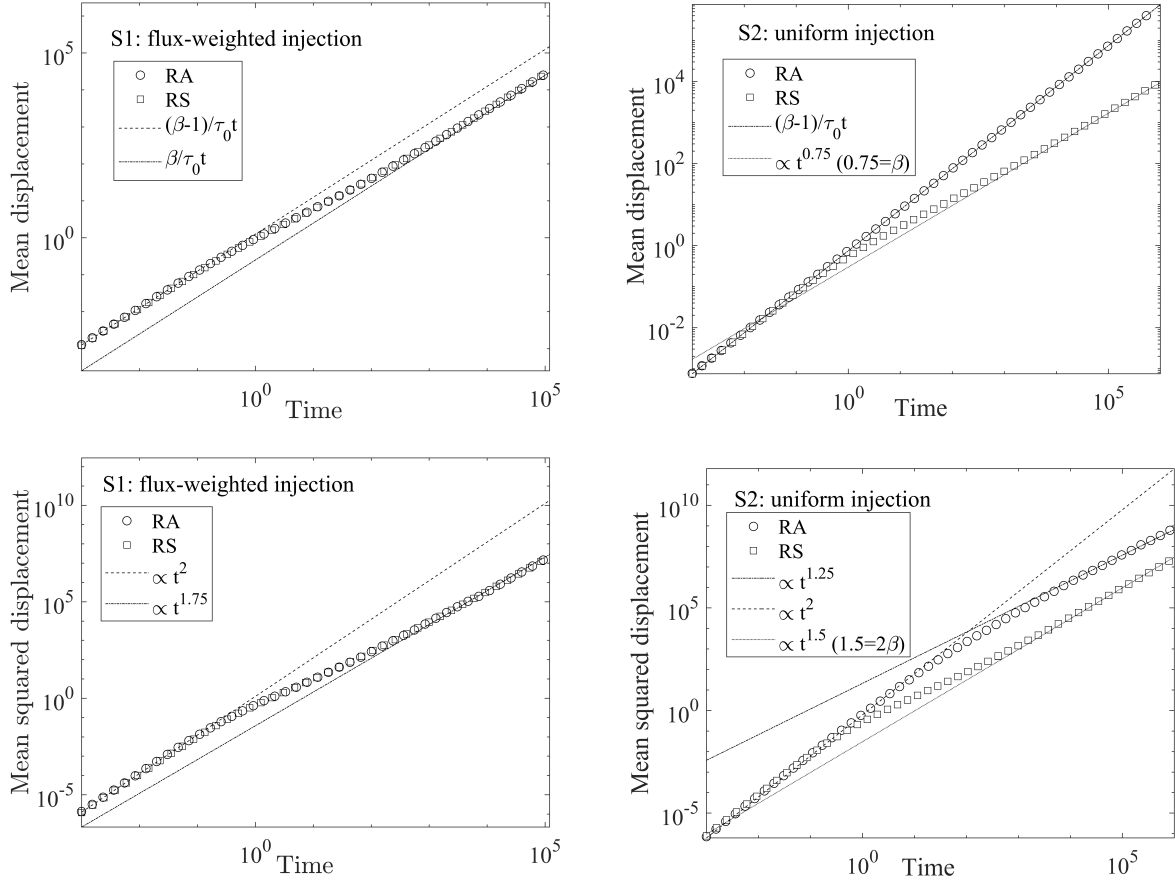


FIG. 2. Displacement (top row) mean and (bottom row) variance for (left) scenario S1 ($\gamma = 1.25$ and $\alpha = 0.25$) under flux-weighted injection, and (right) scenario S2 ($\gamma = 0.75$ and $\alpha = 0.75$) under uniform injection. The squares denote the RS, the circles denote the RA model.

This behavior is due the fact that once particles leave the source zone, they are propagated at higher average velocity in the RA than in the RS model.

2. Displacement mean and variance

We now focus on the temporal evolutions of the displacement mean and variance for RS and RA in the two scenarios S1 and S2. From CTRW theory [25], we expect for the RS model the long-time scalings $m(t) \propto t^\gamma$ and $\kappa(t) \propto t^{2\gamma}$ for $0 < \gamma < 1$ and $m(t) \propto t$ and $\kappa(t) \propto t^{3-\gamma}$ for $1 < \gamma < 2$. For the RA model, we expect $m(t) \propto t$ and $\kappa(t) \propto t^{2-\alpha}$ for $0 < \alpha < 1$. These asymptotic behaviors are reflected in the data for the RS and RA models displayed in Figure 2.

As shown in the top row of Figure 2, the displacement mean evolves for scenarios initially linearly with time, which reflects the correlation of particle velocities on the scale ℓ_c . The displacement mean for the RS and RA models are identical for flux-weighted injection in S1. The mean displacement evolves linearly in time with two different slopes at early and late times, which is a manifestation of aging, that is, the mean velocity evolves in time [41], albeit towards a stationary limit, which is given by the mean flow velocity in the RA model. We call this behavior weak aging because an asymptotic constant velocity exists. The initial velocity is higher than the asymptotic mean due to the flux-weighting in the RA model, while the asymptotic velocity is equal to the mean Eulerian flow velocity. In scenario S2, the mean displacement in the RA and RS models behave in the same way at early times. Here, the RA model does not display aging. Its mean displacement increases linearly with time according to the average flow velocity. The RS model on the other hand, displays aging. Its mean displacement behaves sublinearly as $m(t) \propto t^{3/4}$ due to strong particle retention. We term this behavior here strong aging because there is no asymptotic particle velocity.

As shown in the bottom row of Figure 2, the displacement variances evolve ballistically at early times, that is, according to $\kappa(t) \propto t^2$ for the two scenarios. For S1, the behaviors of RS and RA are identical for flux-weighted injection. At large times, $\kappa(t)$ in both models scale as $t^{1.75}$. For scenario S2 the situation is different. While the displacement variances $\kappa(t)$ behave identically for the RS and RA models at short times, at large times, $\kappa(t) \propto t^{3/2}$ for RS and $\propto t^{5/4}$ for RA. The displacement mean and variance in general behave differently in the RA and RS models depending on the initial conditions even though the early or late time scalings may be similar.

3. Breakthrough curves

In this section, we consider particle breakthrough curves in scenarios S1 and S2 for the RS and RA models at three different controls planes at distances ℓ_c , $10\ell_c$ and $10^2\ell_c$ from the inlet, see Figure 3. For S1 ($\gamma = \alpha + 1$), the breakthrough curves in the RA and RS models are identical as expected. CTRW theory predicts the late time scalings $f(t, x) \propto t^{-1-\gamma}$ for the RS model, and $f(t, x) \propto t^{-2-\alpha}$ for the RA model. For S2 ($\gamma = \alpha$), the breakthrough curves in the RS and RA models have the same late time scalings because the transition time distribution $\psi_0(t) \propto t^{-1-\alpha}$ at the inlet scales in the same way as the transition time

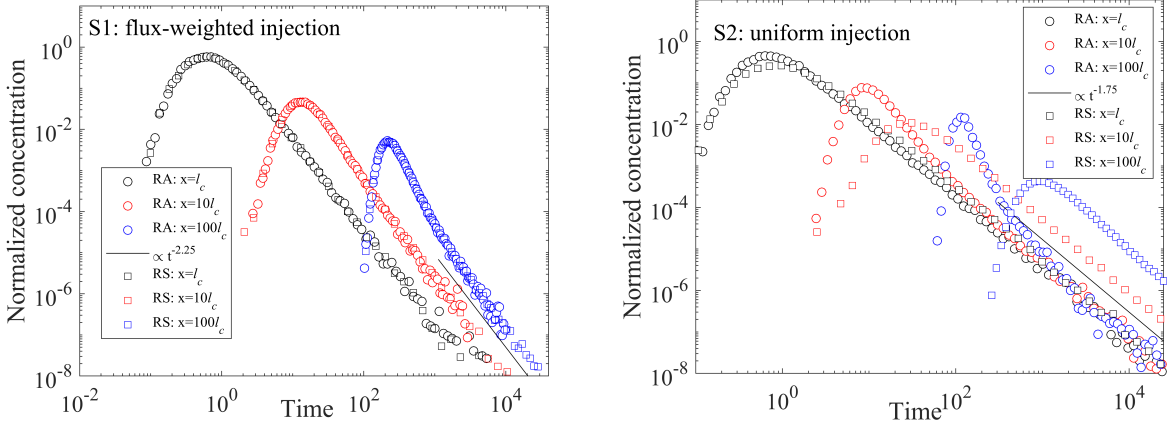


FIG. 3. Breakthrough curves for (left) scenario S1 ($\gamma = 1.25$ and $\alpha = 0.25$) under flux-weighted injection and (right) scenario S2 ($\gamma = 0.75$ and $\alpha = 0.75$) under uniform injection. The squares denote the RS, the circles the RA model.

distribution $\psi(t) \propto t^{-1-\gamma}$ in the RS model. Close to the inlet the breakthrough curves are almost indistinguishable. With increasing distance, however, the peak arrival in the RA model occurs much earlier than in the RS model due to the fast propagation of the bulk of the particle distribution after the initial step. The long-time scaling in the RA model is fully determined by the transition time distribution $\psi_0(t)$ for the first CTRW step, while the bulk behavior is determined by $\psi(t)$. This is in contrast to the RS model, for which particle retention is much stronger as expressed in the transition time distribution $\psi(t) \propto t^{-1-\gamma}$. In fact, the generalized central limit theorem implies that the breakthrough curves for the RS model converge towards a one-sided stable law, see also C. Thus, breakthrough curves in the RS and RA models may show similar late time scalings, but the general behaviors are quite different and depend on the injection conditions.

B. Transport in the RSA model

We now consider solute transport under the combined impact of heterogeneous sorption and flow velocity. We consider the scenarios S1 and S2 for the distributions of the retardation factor and flow speed defined in Section III A. That is, we use the Gamma distribution (43) for $p_e(v)$ and the inverse Gamma distribution (44) for $p_R(r)$. In order to estimate the asymptotic behaviors of the RSA model, we consider the approximation (36) for $\psi(t)$. We

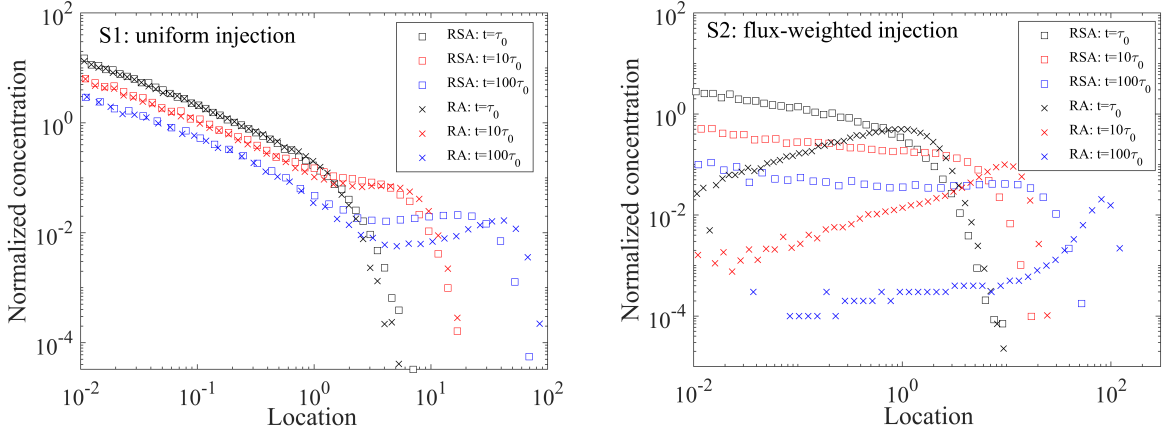


FIG. 4. Spatial particle profiles at time (black) $t = \tau_0$, (red) $t = 10\tau_0$ and (blue) $t = 100\tau_0$ for (left) scenario S1 ($\gamma = 1.25$ and $\alpha = 0.25$) under uniform injection and (right) scenario S2 ($\gamma = 0.75$ and $\alpha = 0.75$) under flux-weighted injection.

find that

$$\psi(t) \propto t^{-1-\beta}, \quad (47)$$

where $\beta = \gamma$ if $\gamma \leq \alpha + 1$ and $\beta = \alpha + 1$ if $\alpha \leq \gamma - 1$, see B. Furthermore, B shows that for uniform injection

$$\psi_0(t) \propto t^{-1-\beta_0}, \quad (48)$$

where $\beta_0 = \gamma$ for $\gamma \leq \alpha$ and $\beta_0 = \alpha$ for $\alpha \leq \gamma$. Under flux-weighted injection, $\beta_0 = \beta$. We consider in the following scenario S1 under uniform injection and scenario S2 under flux-weighted injection. Recall that for S1, $\gamma = \alpha + 1$ and therefore $\beta = \gamma = \alpha + 1$ and $\beta_0 = \alpha$. For S2, $\gamma = \alpha$, which implies that $\beta = \gamma < \alpha + 1$ and $\beta_0 = \gamma = \alpha$.

1. Spatial profiles

The spatial concentration profiles for the RSA and the corresponding profiles for the RA model are shown in Figure 4. For S1, we observe a strong localization of the peak at the origin due to low velocities in the injection region. The peak erodes and a second peak at the leading edge develops. The profiles behave similarly as in the corresponding RA scenario. The concentration profiles for the RSA model here are dominated by velocity heterogeneity.

Variability in the sorption properties manifests in a retardation of the leading edge. Also for S2, we observe peak localization at the origin and the development of a steep leading edge. This behavior, however, is dominated by microscale heterogeneity in the sorption properties. The spatial profiles for the RA scenario behave very differently and are characterized by a tailing tail and a peak at the leading edge. While both random sorption and random advection may cause strong retention at the origin, they manifest differently in the behavior of the leading edge.

2. Displacement mean and variance

Figure 5 shows the displacement mean and variance for S1 under uniform and S2 under flux-weighted injection. For both scenarios, the mean displacement at short times is given by

$$m(t) = \frac{\langle v_0 \rangle t}{R_H}, \quad (49)$$

where $\langle v_0 \rangle$ is the mean initial velocity, and R_H the harmonic mean retardation coefficient.

For scenario S1, $\langle v_0 \rangle = \langle v_e \rangle$, which implies that the ratio of the slopes at early and late times gives the ratio of the arithmetic and harmonic mean retardation coefficients. Transport is retarded compared to the corresponding RA model. The long-time behavior of $m(t)$ in scenario S1 is given by

$$m(t) = \frac{\langle v_e \rangle t}{R_A}, \quad (50)$$

where R_A is the arithmetic mean retardation coefficient. The RSA model displays weak aging, while the mean displacement in the RA model evolves according to the constant mean flow velocity. For scenario S2, the long-time behavior of $m(t)$ scales sublinearly with time according to

$$m(t) \propto t^\gamma. \quad (51)$$

The RSA model is dominated by random sorption and displays strong aging, in contrast to the corresponding RA model.

The displacement variances show at short time the characteristic ballistic behavior, which is given by

$$\sigma^2(t) = [\sigma_{v_0}^2 \langle \mu^2 \rangle + \langle v_0 \rangle^2 \sigma_\mu^2] t^2, \quad (52)$$

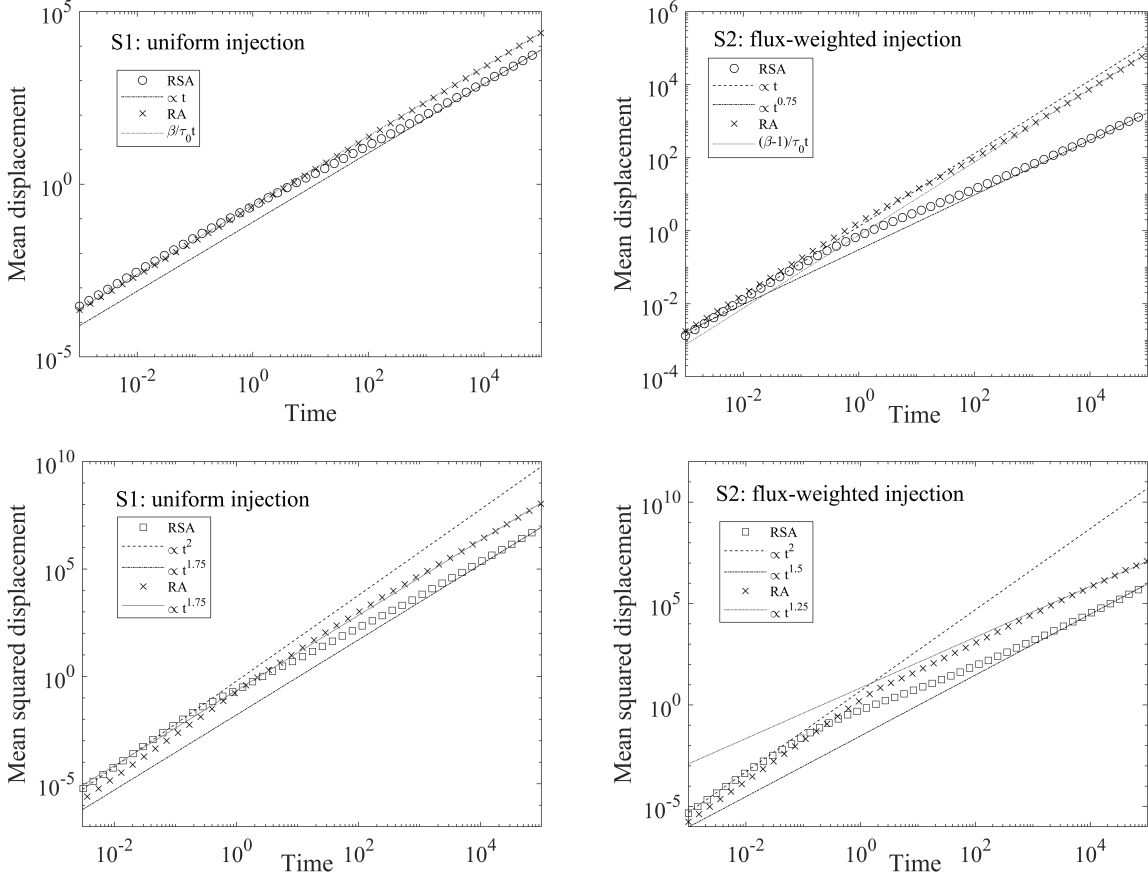


FIG. 5. Mean displacements and displacement variance for (left column) scenario S1 ($\gamma = 1.25$ and $\alpha = 0.25$) under uniform injection and (right column) scenario S2 ($\gamma = 0.75$ and $\alpha = 0.75$) under flux-weighted injection.

where we defined $\mu = 1/R$, and σ_μ^2 is the variance of μ . The long-time scalings are super-linear for both scenarios. Nevertheless, for S1, the long-time behavior is dominated by microscale advection and the scaling is $\sigma^2(t) \propto t^{2-\alpha}$. The evolution is delayed due to the presence of random sorption compared to the corresponding RA model. For scenario S2 the behavior is dominated by microscale retardation and the variance scales as $\sigma^2(t) \propto t^{2\gamma}$.

3. Breakthrough curves

Figure 6 shows the breakthrough for S1 under uniform and S2 and flux-weighted injection. The microscale disorder gives rise to strong tailing in both scenarios. In S1, the tailing is dominated by low flow velocities at the injection point and thus, the long-time scaling is given

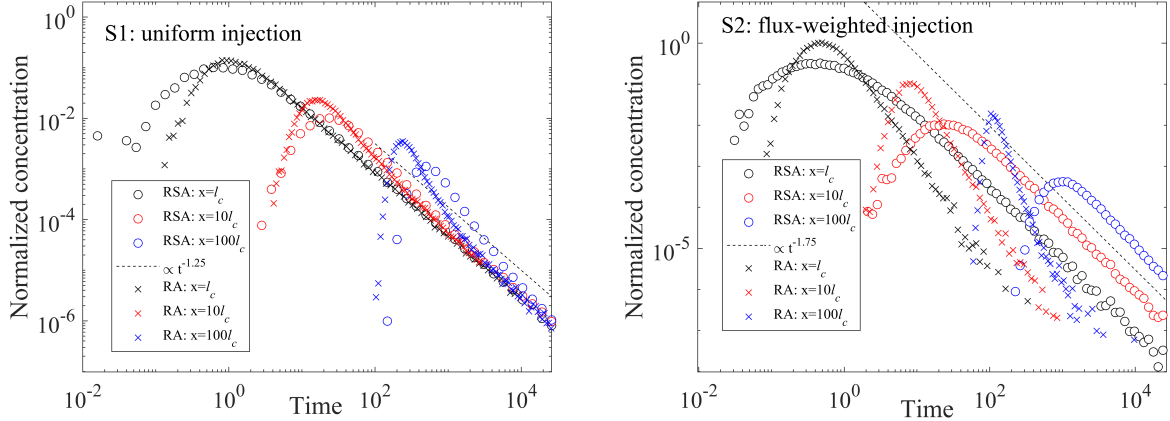


FIG. 6. Breakthrough curves for (left) scenario S1 ($\gamma = 1.25$ and $\alpha = 0.25$) under uniform injection and (right) scenario S2 ($\gamma = 0.75$ and $\alpha = 0.75$) under flux-weighted injection.

by $f(t, x) \propto t^{-1-\alpha}$. The breakthrough curves are similar to the ones for the corresponding RA model, but show a delay in the peak arrival caused by random sorption. For S2, the breakthrough curve is dominated by random sorption. The long-time scaling is $f(t, x) \propto t^{-1-\gamma}$, and very different from the behavior of the corresponding RA model. Nevertheless, from the asymptotic scaling alone it is not possible to distinguish the dominant microscale disorder mechanism.

IV. CONCLUSION

We explore the impact of random sorption, and random advection on large-scale non-Fickian transport using two CTRW models, the RS and RA models, respectively, which explicitly represent these disorder mechanisms. The RS model accounts for instantaneous mobile-immobile mass exchange, which is characterized by a spatially variable retardation coefficient. The RA model quantifies particle transport in media characterized by spatially variable steady flow. Furthermore, we derive the novel RSA model that quantifies the combined effect of the two microscale disorder models and represents transport in a heterogeneous flow field under instantaneous heterogeneous sorption-desorption. We analyze and compare the transport behaviors in the three models for uniform and flux-weighted initial conditions in terms of spatial profiles of the particle density, the displacement mean and variance, and particle breakthrough curves. In order to probe the impact of the mi-

crosscale physics on large-scale dispersion, we consider disorder distributions that give the same power-law transition time distributions in the corresponding CTRW models. Under these conditions, the different microscopic disorder models lead to similar large-scale dispersion behaviors. The RA and RS models differ in their responses to initial particle distributions that are not flux-weighted. While the RS model displays always aging for exponents $0 < \gamma < 1$, [41], that is, the particle velocity is a non-stationary stochastic process, the RA model is stationary for uniform injection conditions, and evolves toward a stationary limit for arbitrary initial particle distributions.

The large-scale dispersion signatures in the three disorder models are similar in that they can lead to forward and backward tails in the spatial particle profiles, superdiffusive growth of the displacement variance, and power-law tails in the particle breakthrough curves. However, while the RA model leads always to superdiffusive behavior, the RS model displays subdiffusive behavior for exponents $0 < \gamma < 1/2$ together with a sublinear scaling of the mean displacement. The spatial profiles can develop double peak behaviors in all models, depending on the microscale disorder distribution for the RS model, and on the injection condition for the RA model. These behaviors are characterized by a localized peak at the origin that erodes with time, and a peak at the leading front. The RA model does not display double peak behavior for flux-weighted injection, but gives a trailing tail and well-defined peak at the front, similar to the RS model for $1 < \gamma < 2$. Under uniform injection, the RA model develops two clearly separated peaks and a fast moving leading edge. The breakthrough curves display power-law scaling $\propto t^{-1-\beta}$ with $0 < \beta < 2$ for all disorder models. The power-law range $0 < \beta < 1$ corresponds in the RS model to the exponents $0 < \gamma < 1$. In this case, the breakthrough curve converges toward a one-sided stable distribution. In the RA model, in contrast, this behavior can only be observed for uniform injection, and the breakthrough curve does not converge to a stable distribution. In this case, the tail behavior is fully determined by the transition time distribution for the first CTRW step, and the peak arrival is much earlier than in the RS model with the same tailing behavior.

In conclusion, while the large-scale signatures of dispersion in the disorder models under consideration are similar, their responses to initial particle distributions that are not flux-weighted can be very different. Thus, under certain conditions, it is possible to infer the microscale physics from the observation of the dispersion behavior. A CTRW model

with power-law transition time distribution in general allows to reproduce anomalous dispersion as manifest in non-linear scalings of displacement mean and variance, and power-law tails in particle breakthrough curve. However, it is important to identify and characterize the microscale physics and disorder properties to be able to predict the large scale system behaviors.

ACKNOWLEDGEMENT

X.Y. acknowledges the support by National Natural Science Foundation of China (U2267218 and 11972148) and the China Scholarship Council under Grant No. 202006710018. M.D. acknowledges the support of MCIN/AEI/10.13039/501100011033 through Grant CEX2018-000794-S and funding by the European Union (ERC, KARST, 101071836). Y.Z. acknowledges the support by the U.S. National Science Foundation (Grant No. 2305141). Any opinions, findings, conclusions, or recommendations do not necessarily reflect the views of these funding agencies.

Appendix A: Boltzmann equation for the RSA model

The joint distribution $p(x, v, r, t)$ of particle position, velocity and retardation coefficient can be written as

$$p(x, v, r, t) = \frac{r}{v} \int_0^\infty ds \langle \delta[x - x(s)] \delta[v - v(s)] \delta[r - r(s)] \delta[t - t(s)] \rangle \quad (\text{A1})$$

$$\equiv \frac{r}{v} \int_0^\infty ds \Pi(x, v, r, t, s) \quad (\text{A2})$$

The derivative of $\Pi(x, v, r, t, s)$ along s is given by particle conservation as

$$\begin{aligned} \frac{\partial \Pi(x, v, r, t, s)}{\partial s} = & -\frac{\partial \Pi(x, v, r, t, s)}{\partial x} + \frac{D}{v} \frac{\partial^2 \Pi(x, v, r, t, s)}{\partial x^2} - \frac{r}{v} \frac{\partial \Pi(x, v, r, t, s)}{\partial t} \\ & + \frac{1}{\ell_c} \int_0^\infty dv' \int_0^\infty dr' p_v(v) \psi_R(r) \Pi(x, v', r', t, s) - \frac{1}{\ell_c} \Pi(x, v, r, t, s) \end{aligned} \quad (\text{A3})$$

Integration of the latter over s according to Eq. (A2) gives Eq. (33).

Appendix B: Scaling of transition time distribution for the RSA model

The transition time distribution of the RSA model can be written as

$$\psi(t) = \int_0^\infty dr \int_0^\infty dv \delta\left(t - \frac{\ell_c r}{v}\right) p_R(r) p_v(v), \quad (\text{B1})$$

where $\delta(x)$ denotes the Dirac Delta. Using that $\delta(ax) = \frac{1}{|a|}\delta(x)$, we obtain Eq. (36). We use expression (44) for $p_R(r)$ and for $p_v(v)$, we use expression (43) for $p_e(v)$ in definition (19) for $p_v(v)$ to obtain

$$p_v(v) = \left(\frac{v}{v_0}\right)^\alpha \frac{\exp(-v/v_0)}{v_0 \Gamma(\alpha + 1)} \quad (\text{B2})$$

Using these expressions in Eq. (36) we obtain

$$\psi(t) = \int_0^\infty dv \frac{v}{\ell_c} \left(\frac{vt}{\ell_c r_0}\right)^{-\gamma-1} \frac{e^{-\frac{\ell_c r_0}{vt}}}{r_0 \Gamma(\gamma)} \left(\frac{v}{v_0}\right)^\alpha \frac{e^{-\frac{v}{v_0}}}{v_0 \Gamma(\alpha + 1)}, \quad (\text{B3})$$

For $\gamma < \alpha + 1$ and $t \gg \ell_c r_0 / v_0$, Eq. (B3) can be approximated as

$$\psi(t) = \left(\frac{v_0 t}{\ell_c r_0}\right)^{-1-\gamma} \frac{v_0}{\ell_c r_0} \int_0^\infty dv \left(\frac{v}{v_0}\right)^{\alpha-\gamma} \frac{e^{-\frac{v}{v_0}}}{\Gamma(\gamma) \Gamma(\alpha + 1) v_0}, \quad (\text{B4})$$

where we used that $e^{-\frac{\ell_c r_0}{vt}} \rightarrow 1$ for $t \gg \ell_c r_0 / v_0$. Evaluating the integral on the right side, we obtain

$$\psi(t) = \left(\frac{v_0 t}{\ell_c r_0}\right)^{-1-\gamma} \frac{v_0}{\ell_c r_0} \frac{\Gamma(\alpha - \gamma + 1)}{\Gamma(\gamma) \Gamma(\alpha + 1)}, \quad (\text{B5})$$

For $\alpha < \gamma - 1$, we perform the variable transform $v \rightarrow \ell = vt/r_0$ in (B3), which gives

$$\psi(t) = \left(\frac{v_0 t}{\ell_c r_0}\right)^{-\alpha-2} \frac{v_0}{\ell_c r_0} \int_0^\infty d\ell \left(\frac{\ell}{\ell_c}\right)^{-(\gamma-\alpha-1)-1} \frac{e^{-\frac{\ell_c}{\ell}}}{\Gamma(\gamma)} \frac{e^{-\frac{\ell r_0}{v_0 t}}}{\Gamma(\alpha + 1)}. \quad (\text{B6})$$

In the limit $t \gg \ell_c r_0 / v_0$, the integral on the right side can be evaluated explicitly, which gives

$$\psi(t) = \left(\frac{v_0 t}{\ell_c r_0}\right)^{-\alpha-2} \frac{v_0}{\ell_c r_0} \frac{\Gamma(\gamma - \alpha - 1)}{\Gamma(\gamma) \Gamma(\alpha + 1)}. \quad (\text{B7})$$

For $\psi_0(t)$ in the case of uniform injection, the derivations are analogous. For $\gamma < \alpha$, we obtain

$$\psi_0(t) = \left(\frac{v_0 t}{\ell_c r_0}\right)^{-1-\gamma} \frac{v_0}{\ell_c r_0} \frac{\Gamma(\alpha - \gamma)}{\Gamma(\gamma) \Gamma(\alpha)}, \quad (\text{B8})$$

For $\alpha < \gamma$, we obtain

$$\psi_0(t) = \left(\frac{v_0 t}{\ell_c r_0}\right)^{-\alpha-1} \frac{v_0}{\ell_c r_0} \frac{\Gamma(\gamma - \alpha)}{\Gamma(\gamma) \Gamma(\alpha)}. \quad (\text{B9})$$

Appendix C: One-sided stable distribution in the RS model

We discuss the convergence of the particle breakthrough curves toward a one-sided stable law with distance of the control plane in the RS model. To this end, we consider the particle arrival time in the corresponding CTRW model (9) for the constant transition length $\xi = \ell_c$. Thus, the arrival t_n at a control plane at distance $x_n = n\ell_c$ from the inlet is

$$t_n = \sum_{n=1}^n \tau_n, \quad (\text{C1})$$

where the transition times τ_n are distributed according to the heavy-tailed $\psi(t) \propto t^{-1-\gamma}$ for $0 < \gamma < 1$. According to the generalized central limit theory, the distribution t_n converges toward a one-sided stable distribution [42].

-
- [1] B. Bijeljic, P. Mostaghimi, and M. J. Blunt, “Signature of non-Fickian solute transport in complex heterogeneous porous media,” *Phys. Rev. Lett.* **107**, 204502 (2011).
 - [2] Pietro De Anna, Tanguy Le Borgne, Marco Dentz, Alexandre M Tartakovsky, Diogo Bolster, and Philippe Davy, “Flow intermittency, dispersion, and correlated continuous time random walks in porous media,” *Physical Review Letters* **110**, 184502 (2013).
 - [3] P. K. Kang, P. de Anna, J.P. Nunes, B. Bijeljic, M. J. Blunt, and R. Juanes, “Pore-scale intermittent velocity structure underpinning anomalous transport through 3-d porous media,” *Geophys. Res. Lett.* **41** (17), 6184–6190 (2014).
 - [4] Veronica L Morales, Marco Dentz, Matthias Willmann, and Markus Holzner, “Stochastic dynamics of intermittent pore-scale particle motion in three-dimensional porous media: Experiments and theory,” *Geophysical Research Letters* **44**, 9361–9371 (2017).
 - [5] Alexandre Puyguraud, Philippe Gouze, and Marco Dentz, “Upscaling of anomalous pore-scale dispersion,” *Transport in Porous Media* **128**, 837–855 (2019).
 - [6] E. E. Adams and L. W. Gelhar, “Field study of dispersion in a heterogeneous aquifer 2. spatial moment analysis,” *Water Resour. Res.* **28**, 3293–3307 (1992).
 - [7] Charles Harvey and Steven M Gorelick, “Rate-limited mass transfer or macrodispersion: Which dominates plume evolution at the macrodispersion experiment (made) site?” *Water Resources Research* **36**, 637–650 (2000).

- [8] David A Benson, Rina Schumer, Mark M Meerschaert, and Stephen W Wheatcraft, “Fractional dispersion, lévy motion, and the made tracer tests,” *Transport in porous media* **42**, 211–240 (2001).
- [9] Yong Zhang, Mark M Meerschaert, Boris Baeumer, and Eric M LaBolle, “Modeling mixed retention and early arrivals in multidimensional heterogeneous media using an explicit lagrangian scheme,” *Water Resources Research* **51**, 6311–6337 (2015).
- [10] HongGuang Sun, Dong Chen, Yong Zhang, and Li Chen, “Understanding partial bed-load transport: Experiments and stochastic model analysis,” *Journal of Hydrology* **521**, 196–204 (2015).
- [11] Alessandro Comolli, Vivien Hakoun, and Marco Dentz, “Mechanisms, upscaling, and prediction of anomalous dispersion in heterogeneous porous media,” *Water Resources Research* **55**, 8197–8222 (2019).
- [12] Roy Haggerty, Sean W Fleming, Lucy C Meigs, and Sean A McKenna, “Tracer tests in a fractured dolomite: 2. analysis of mass transfer in single-well injection-withdrawal tests,” *Water Resources Research* **37**, 1129–1142 (2001).
- [13] M. W. Becker and A. M Shapiro, “Interpreting tracer breakthrough tailing from different forced-gradient tracer experiment configurations in fractured bedrock,” *Water Resour. Res.* **39** (2003).
- [14] Peter K Kang, Tanguy Le Borgne, Marco Dentz, Olivier Bour, and Ruben Juanes, “Impact of velocity correlation and distribution on transport in fractured media: Field evidence and theoretical model,” *Water Resources Research* **51**, 940–959 (2015).
- [15] Seonkyoo Yoon and Peter K Kang, “Roughness, inertia, and diffusion effects on anomalous transport in rough channel flows,” *Physical Review Fluids* **6**, 014502 (2021).
- [16] Peter Nkedi-Kizza, P Suresh Chandra Rao, and Arthur G Hornsby, “Influence of organic cosolvents on sorption of hydrophobic organic chemicals by soils,” *Environmental science & technology* **19**, 975–979 (1985).
- [17] Xuan Han, Yong Zhang, Chunmiao Zheng, Xiangnan Yu, Shiyin Li, and Wei Wei, “Enhanced cr (vi) removal from water using a green synthesized nanocrystalline chlorapatite: Physicochemical interpretations and fixed-bed column mathematical model study,” *Chemosphere* **264**, 128421 (2021).

- [18] KH Coats and BD Smith, “Dead-end pore volume and dispersion in porous media,” *Society of petroleum engineers journal* **4**, 73–84 (1964).
- [19] Roy Haggerty and Steven M Gorelick, “Multiple-rate mass transfer for modeling diffusion and surface reactions in media with pore-scale heterogeneity,” *Water Resources Research* **31**, 2383–2400 (1995).
- [20] Marco Dentz, Peter K Kang, Alessandro Comolli, Tanguy Le Borgne, and Daniel R Lester, “Continuous time random walks for the evolution of lagrangian velocities,” *Physical Review Fluids* **1**, 074004 (2016).
- [21] Christopher Green, “Connected-network paradigm for the alluvial aquifer system,” *Theory, Modeling, and Field Investigation in Hydrogeology: A Special Volume in Honor of Shlomo P. Neuman’s 60th Birthday* **348**, 25 (2000).
- [22] Chunmiao Zheng and Steven M Gorelick, “Analysis of solute transport in flow fields influenced by preferential flowpaths at the decimeter scale,” *Groundwater* **41**, 142–155 (2003).
- [23] Benoit Noetinger, Delphine Roubinet, Anna Russian, Tanguy Le Borgne, Frederick Delay, Marco Dentz, Jean-Raynald De Dreuzy, and Philippe Gouze, “Random walk methods for modeling hydrodynamic transport in porous and fractured media from pore to reservoir scale,” *Transport in Porous Media* **115**, 345–385 (2016).
- [24] Christophe C Fripiat and Alain E Holeyman, “A comparative review of upscaling methods for solute transport in heterogeneous porous media,” *Journal of Hydrology* **362**, 150–176 (2008).
- [25] Brian Berkowitz, Andrea Cortis, Marco Dentz, and Harvey Scher, “Modeling non-fickian transport in geological formations as a continuous time random walk,” *Reviews of Geophysics* **44** (2006).
- [26] Shlomo P Neuman and Daniel M Tartakovsky, “Perspective on theories of non-fickian transport in heterogeneous media,” *Advances in Water Resources* **32**, 670–680 (2009).
- [27] John H Cushman and Tim R Ginn, “Fractional advection-dispersion equation: A classical mass balance with convolution-fickian flux,” *Water resources research* **36**, 3763–3766 (2000).
- [28] Xiaoxian Zhang, John W Crawford, Lynda K Deeks, Marc I Stutter, A Glyn Bengough, and Iain M Young, “A mass balance based numerical method for the fractional advection-dispersion equation: Theory and application,” *Water resources research* **41** (2005).
- [29] Rina Schumer, David A Benson, Mark M Meerschaert, and Boris Baeumer, “Fractal mobile/immobile solute transport,” *Water Resources Research* **39** (2003).

- [30] Frédéric Delay and Jacques Bodin, “Time domain random walk method to simulate transport by advection-dispersion and matrix diffusion in fracture networks,” *Geophysical Research Letters* **28**, 4051–4054 (2001).
- [31] Vladimir Cvetkovic, Aldo Fiori, and Gedeon Dagan, “Solute transport in aquifers of arbitrary variability: A time-domain random walk formulation,” *Water Resources Research* **50**, 5759–5773 (2014).
- [32] Brian Berkowitz and Harvey Scher, “Anomalous transport in random fracture networks,” *Physical review letters* **79**, 4038 (1997).
- [33] J. D. Hyman, M. Dentz, A. Hagberg, and P. Kang, “Linking structural and transport properties in three-dimensional fracture networks,” *J. Geophys. Res.-Sol. Ea.* (2019).
- [34] Marco Dentz and Adolfo Castro, “Effective transport dynamics in porous media with heterogeneous retardation properties,” *Geophysical Research Letters* **36** (2009).
- [35] Mark L Brusseau, “Transport of reactive contaminants in heterogeneous porous media,” *Reviews of Geophysics* **32**, 285–313 (1994).
- [36] Peter K Kang, Marco Dentz, Tanguy Le Borgne, Seunghak Lee, and Ruben Juanes, “Anomalous transport in disordered fracture networks: Spatial markov model for dispersion with variable injection modes,” *Advances in Water Resources* **106**, 80–94 (2017).
- [37] Tomás Aquino and Andrés Velásquez-Parra, “Impact of velocity correlations on longitudinal dispersion in space-lagrangian advective transport models,” *Physical Review Fluids* **7**, 024501 (2022).
- [38] George Demmy, Sten Berglund, and Wendy Graham, “Injection mode implications for solute transport in porous media: Analysis in a stochastic lagrangian framework,” *Water resources research* **35**, 1965–1973 (1999).
- [39] JD Hyman, Scott L Painter, Hari Viswanathan, Nataliia Makedonska, and Satish Karra, “Influence of injection mode on transport properties in kilometer-scale three-dimensional discrete fracture networks,” *Water Resources Research* **51**, 7289–7308 (2015).
- [40] Igor Janković and Aldo Fiori, “Analysis of the impact of injection mode in transport through strongly heterogeneous aquifers,” *Advances in Water Resources* **33**, 1199–1205 (2010).
- [41] Igor M Sokolov, “Models of anomalous diffusion in crowded environments,” *Soft Matter* **8**, 9043–9052 (2012).

- [42] Vladimir V Uchaikin and Vladimir M Zolotarev, *Chance and stability: stable distributions and their applications* (Walter de Gruyter, 1999).